Aljawad, Murtada Saleh; Schwalbert, Mateus Palharini; Mahmoud, Mohamed; Sultan, Abdullah

Article

Impacts of natural fractures on acid fracture design: A modeling study

Energy Reports

Provided in Cooperation with:
Elsevier

Suggested Citation: Aljawad, Murtada Saleh; Schwalbert, Mateus Palharini; Mahmoud, Mohamed; Sultan, Abdullah (2020) : Impacts of natural fractures on acid fracture design: A modeling study, Energy Reports, ISSN 2352-4847, Elsevier, Amsterdam, Vol. 6, pp. 1073-1082, https://doi.org/10.1016/j.egyr.2020.04.030

Energy Reports 6 (2020) 1073–1082

Contents lists available at ScienceDirect

Energy Reports

journal homepage: www.elsevier.com/locate/egyr

Research paper

Impacts of natural fractures on acid fracture design: A modeling study

Murtada Saleh Aljawad [a,*], Mateus Palharini Schwalbert [b], Mohamed Mahmoud [a], Abdullah Sultan [a]

[a] College of Petroleum Engineering and Geosciences, KFUPM, Dhahran, 31261, Saudi Arabia
[b] Petrobras, Rio de Janeiro RJ, 20930-040, Brazil

ARTICLE INFO

Article history:
Received 6 February 2020
Received in revised form 18 April 2020
Accepted 21 April 2020
Available online xxxx

ABSTRACT

Carbonate formations, which are usually naturally fractured, are good candidates for acid fracturing. Natural fractures have a significant impact on the execution and outcomes of acid fracture design. The interaction of hydraulics with natural fractures can be complex and is rarely considered in acid fracture modeling. This study provides an integrated approach where natural fractures are considered in both acid fracture and productivity modeling. The model is dynamic, integrating fracture propagation with reactive acid transport and coupled with heat transfer. The proposed acid fracture model generates fracture network permeability, which is then used in the productivity model.

A parametric study was conducted to investigate the impact of natural fractures on the productivity of acid fractured wells. Multiple scenarios of different natural fracture spacings, lengths, and widths were investigated. It was determined that the existence of natural fractures negatively impacted productivity because they limited the extension of the hydraulic fracture. The impact was found to be more significant when the reservoir was tight, situations where a long hydraulic fracture is desirable. It was also found that the optimum acid injection rate increased with an increase in natural fracture intensity at moderate reservoir permeability levels. Nevertheless, the maximum injection rate should be targeted in tight formations, no matter the intensity of the natural fracture. Implementation of diversion stages could significantly improve the productivity of an acid fractured well.

1. Introduction

Acid fracturing is a well stimulation technique applied to tight carbonate reservoirs to enhance hydrocarbon production. Acid etches fracture surfaces in irregular patterns, resulting in a conductive fracture and eliminating the need for proppant. A treatment design consists of multiple stages that could be repeated in cycles. Usually, each cycle contains a hydrochloric acid (HCl) stage and diverter. Treatment begins with a pad (i.e., non-reactive) fluid to initiate and propagate the fracture and ends with a water flush to clean the tubular and push the acid from the near-wellbore region (Li et al., 1993; Aljawad et al., 2019a).

Acid fracturing could be compared to matrix acidizing, which is another stimulation method that requires injection below fracturing pressure. Matrix acidizing is frequently performed for near-wellbore cleaning and productivity enhancement. Deciding to simulate a well with acid fracturing or matrix acidizing can be challenging. Schwalbert (2019) showed through simulations that acid fracturing results in better productivity than does matrix acidizing below a certain cutoff permeability. This permeability can be estimated based on the formation and acid properties. Palharini Schwalbert et al. (2020) provided a formula to estimate the cutoff permeability, with a methodology based on the rock type and strength, formation depth, and treatment volume. Acid fracturing is a less promising method when the fracture height could grow to the surrounding water aquifers or gas caps.

Propped fracturing is another stimulation method wherein proppant slurry is used instead of acid. Abass et al. (2006) showed experimentally that propped fractures could be better at maintaining the hydraulic fracture conductivity at higher closure stresses. However, acid fracturing is a less expensive option and proppant screenout is not an issue. Acid fracturing could perform better in shallow heterogeneous formations, as well as in formations containing natural fractures, mainly if the proppant screenout challenge is a possible outcome.

Conductivity and acid penetration length are the factors that control the fractured well productivity according to previous research. These two factors can be designed to achieve optimum productivity from an acid fracture job. However, research targeting acid fracture design optimization is limited. Sevougian et al. (1987) started early research targeting acid fracture design optimization. They formulated a solution for the optimum conductivity and acid penetration length. The study concluded that

* Corresponding author.
E-mail address: mjawad@kfupm.edu.sa (M.S. Aljawad).

https://doi.org/10.1016/j.egyr.2020.04.030

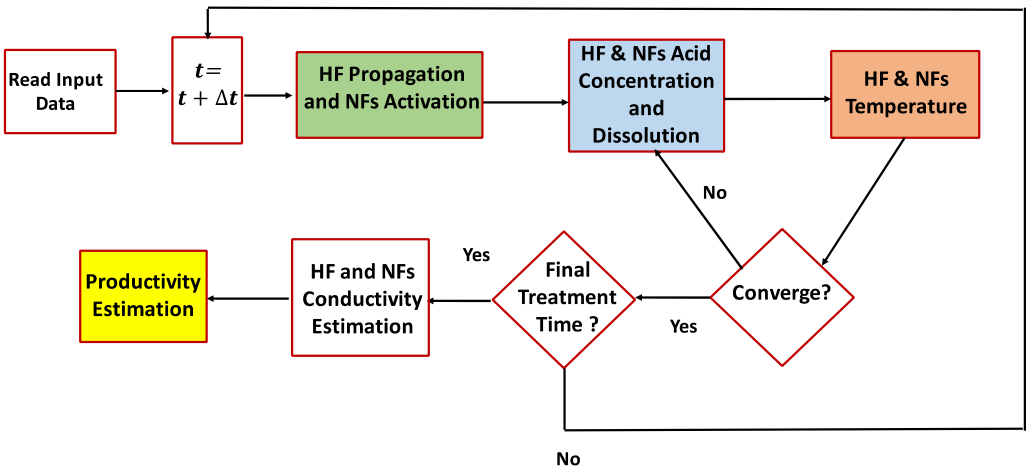

Fig. 1. Workflow showing the methodology of coupling acid fracture and reservoir model.

a Peclet number of 4 should be designed to achieve optimum productivity. The unified fracture design (UFD) approach was applied by Ravikumar et al. (2015) to optimize acid fracture design. Lately, Aljawad et al. (2019b) illustrated that the optimum acid fracture design is a function of formation permeability, rock mineralogy, depth, rock strength, and acid treatment volume. For instance, low to moderate injection rates should be targeted in relatively high permeability formations, while the maximum injection rate should be achieved in tight reservoirs. The optimum design could be accomplished through different design conditions. Increasing the acid treatment volume requires a higher optimum acid injection rate. Also, minerals with lower levels of reactivity (e.g., dolomite) have lower optimal injection rates compared to calcite formations.

Considering the existence of natural fractures (NFs) in acid fracture modeling is essential to optimizing the design. There are only a few studies that have considered the impact of NFs. In 2016, Mou et al. provided a model that captures acid fracture leakoff when applied to naturally fractured formations. Those researchers observed that most leakoff occurred in the NFs, while leakoff in the matrix was negligible. Ugursal et al. (2018) studied the impact of NFs on acid fracture design and productivity estimation. Their model assumed a constant hydraulic fracture (HF) length despite the number of NFs. Such an assumption was not valid, as NFs are known to limit HF propagation. NFs can either enhance or reduce the productivity of an acid fractured well based on their intensity according to Ugursal et al.'s study.

The present study developed an acid fracture model that considers the existence of NFs. The model is dynamic where the HF propagates, and activates NFs along the way, an approach that has not been considered previously in acid fracture modeling. Numerical acid and heat transfer models are solved along the HF and NFs; the numerical productivity model considers the existence of NFs as the reservoir fluids are produced. This work shows that NFs changes the acid distribution in the reservoir and hence, significantly alter the design outcomes.

2. Methodology

The model presented by Aljawad et al. (2019b, 2020) served as the basis for solving the acid-reactive transport and resulting productivity. The previous work modeled the mass and heat transfer in a propagating HF only. This research, however, considered the impact of NFs on HF propagation, acid and temperature distribution, and productivity estimation. This is a significant addition as NFs are naturally abundant in carbonate formations. An acid fracture model would not be accurate without considering their impacts. The model consists of a coupled acid fracture and reservoir production models. Fig. 1 shows the algorithm of the model, which was developed in-house. At each time step, a HF propagation model that considers the existence of NFs is solved. Then, a coupled mass and heat transfer model is used to obtain the acid concentration and temperature profiles in the system containing one HF and several NFs. The dissolution profile is estimated based on the distribution of acid concentration within the fractures. After reaching the final treatment time, the conductivity of the fracture network is estimated and converted into permeability distribution. This is then exported to the built-in reservoir model to estimate the acid fractured well productivity.

The acid fracture model includes a simplified fracture propagation model that considers the impact of NFs. The assumption is that NFs will be orthogonal to the HF and equally spaced. It should be noted that the interactions between the HF and NFs are complex and depends on many parameters such as the HF/NF angle, stress contrast, fracture pressure magnitude, tensile strength, and NF friction coefficient (Agrawal et al., 2019). Different propagation modes could be encountered as the HF is encountering NFs such as arresting, jogging, branching, and crossing (Potluri et al., 2005). It is assumed in this study that the HF crosses and dilates the NFs (see Fig. 2). According to Potluri et al., this could happen if the followings are satisfied:

$$p_f(t = 0, x = x_{nf}) > \sigma_{n,nf} \tag{1}$$

$$p_f\left(t, x = x_{nf}\right) > \sigma_{h,min} + T_{nf} \tag{2}$$

where p_f is the fracture pressure, $\sigma_{n,nf}$ is the normal stress acting on the NFs surfaces, T_{nf} is the tensile strength of the rock at the intersection, $\sigma_{h,min}$ is the minimum stress horizontal stress, and x_{nf} is the location of a NF. Eq. (1) states that for the NFs to be dilated, the fracture pressure at the time of intersection should be larger than the normal stress acting to close the NFs. Eq. (2) states that for the HF to cross a NF instead of branching, the fracture pressure should exceed the pressure required to re-initiate the HF along the original direction. The normal stress acting on the NFs surface can be defined as:

$$\sigma_{n,nf} = \frac{\sigma_{H,max} + \sigma_{h,min}}{2} + \frac{\sigma_{H,max} - \sigma_{h,min}}{2} Cos(180 - 2\theta) \tag{3}$$

where $\sigma_{H,max}$ is the maximum horizontal stress and θ is the intersection angle between the HF and NFs. Looking at Eqs. (1) and (3), it could be observed that lower angle and stress contrast gives a higher probability of NF dilation. For orthogonal NFs, the normal stress acting on the NFs is the maximum horizontal stress

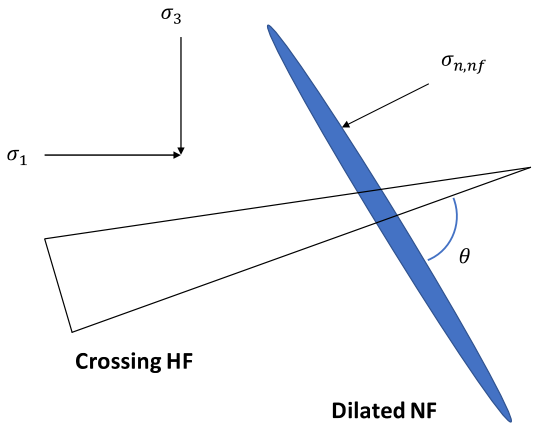

Fig. 2. HF crosses and dilate a NF according to the developed model assumptions.

which improves the possibility of the HF crossing the NFs with no dilation. Nevertheless, NFs will be dilated when a small stress contrast exists; the model assumes that $\sigma_{H,max}$ is only 20% larger than $\sigma_{h,min}$.

According to the above-mentioned assumptions, the HF grows, while the NFs are dilated as being crossed by the HF (i.e., constant dimensions). The fracture propagation model is pseudo-three dimensional (P3D) and used to estimate the average HF length, height, and width (i.e., griddles). The fracture domain, however, is gridded to solve for the acid concentration, temperature, rock dissolution, and well productivity thereafter using the finite volume scheme.

HF length is obtained by solving the material balance equation, presented as:

$$\frac{\partial q}{\partial x} + (q_{L,m} + q_{L,nf}) + \frac{\partial A_c}{\partial t} = 0 \tag{4}$$

where q is the flow rate, x is the location along the fracture length, $q_{L,m}$ is the fluid loss rate in the matrix surrounding the HF per unit length, $q_{L,nf}$ is the NF fluid loss rate per unit length, A_c is the HF cross-sectional area, and t is time. The first term in the above equation is the fluid convection, the second term is the fluid loss through matrix and NFs, the third term is the fluid accumulation in the HF. Notice that the NFs were accounted for in the fracture propagation model through the fluid loss in the material balance equation. In this study, Carter's analytical solution was assumed to be sufficient in estimating the fluid loss. Hill et al.'s (1995) approach was used to account for the excessive fluid loss due to the wormholes growing from the fracture faces which occurs due to acid reaction. Carters and Hill et al. models are described as follows:

$$q_L = \frac{2C_L h_f}{\sqrt{t - \tau\,(x)}} \tag{5}$$

$$C_L = \frac{-\frac{1}{C_c} + \sqrt{\frac{1}{C_c^2} + \frac{4}{C_{v,wh}^2}}}{2\left(\frac{1}{C_{v,wh}^2}\right)} \tag{6}$$

where C_L is the total leakoff coefficient, h_f is the fracture height, $\tau\,(x)$ is the time when the fracture reaches Position x, C_c is the leakoff coefficient accounting for the uninvaded reservoir zone, and $C_{v,wh}$ is the leakoff coefficient of the wormholed region. Eq. (6) is applicable only if the pore volume to breakthrough (PV_{bt}) is larger than one which is assumed in this study. If the PV_{bt} is less than one (i.e., efficient wormholing), the leakoff model provided by Schwalbert (2019) should be implemented. Notice that Eqs. (5) and (6) are applied for both HF and NFs. For the NFs case, t represents the total time the NF was dilated while it represents the total injection time for the HF case. Notice that the NFs are instantaneously dilated (considered in the simulations) once the HF reaches the intersection point. The material balance equation was solved by integrating it with respect to time and space. The cumulative fluid loss from the matrix surrounding the HF, $Q_{L,m}$, as a function of time and position (for one HF wing) is written as:

$$Q_{L,m}(x,t) = \kappa\left(2xh_f\right) C_L\sqrt{t} \tag{7}$$

where the κ is the opening time distribution factor that considers the time-dependent growth of the HF. The cumulative leakoff through one NF, $Q_{L,nf}(t)$, is written as:

$$Q_{L,nf}\left(t > t_{nf}\right) = \left(4L_{nf}h_f\right) C_L\sqrt{t} + 2L_{nf}h_{nf}w_{nf} \tag{8}$$

where L_{nf} is the NF half-length, w_{nf} is the NF width, h_{nf} is the NF height, and t_{nf} is the dilation time of the NF. The κ factor is omitted from Eq. (8) as an instantaneous dilation of NF is assumed ($\tau\,(x) = 0$). Notice that the fluid loss from the NF is composed of time-dependent fluid loss (first term) and instantaneous fluid loss terms (second term). The time-dependent term is accounting for the fluid loss from the NFs to the surrounding matrix. The instantaneous fluid loss term is accounting for the sudden dilation of NFs.

Estimating the HF's width considering the interactions with NFs is complex from geomechanical perspective. Displacement discontinuity method (DDM) is usually applied to describe the hydraulic fracturing opening and interactions (Wu and Olson, 2016). A simplified model is used to estimate the HF dynamic width in this study; assuming it does not change the study outcomes. The HF width (PKN) is obtained through the equation below:

$$w_{w,0} = 9.15^{\frac{1}{2n+2}}\, 3.98^{\frac{n}{2n+2}} \left(\frac{1+2.14n}{n}\right)^{\frac{n}{2n+2}} K^{\frac{1}{2n+2}} \times \left(\frac{q_i^n h_f^{1-n} x_f}{\grave{E}}\right)^{\frac{1}{2n+2}} \tag{9}$$

where $w_{w,0}$ is the HF width, K is the flow consistency index, n is the flow behavior index, $\grave{E}$ is the plain strain modulus, and q_i is the injection rate. The fracture height for multi-layer formation grows if the stress intensity factor, K_I, exceeds the bounding layers toughness. The stress intensity factor can be evaluated as follows (Liu and Valkó, 2018):

$$K_{I+} = \frac{1}{\sqrt{\pi c}} \int_{-c}^{+c} P_n\,(z) \sqrt{\frac{c+z}{c-z}}\, dz \tag{10}$$

$$K_{I-} = \frac{1}{\sqrt{\pi c}} \int_{-c}^{+c} P_n\,(z) \sqrt{\frac{c-z}{c+z}}\, dz \tag{11}$$

where c is the fracture half-height, P_n is the net fracture pressure, z is direction of the fracture height, the subscript $(+)$ refers to the lower tip, and $(-)$ refers to the upper tip. The model assumes that only the HF grows in height while the NFs height is constant and equal to pay zone thickness. Notice that the NFs were accounted for in the model from a material balance perspective and not from geomechanical one.

The fluid velocity distribution inside the hydraulic and natural fracture can be obtained by solving the continuity and momentum balance equations using Berman (1953) approach:

$$\nabla.\boldsymbol{u} = 0 \tag{12}$$

$$\rho_f(\boldsymbol{u}.\nabla\boldsymbol{u}) = -\nabla p + \mu\Delta\boldsymbol{u} \tag{13}$$

where $\boldsymbol{u}$ is the velocity vector, μ is the fracture fluid viscosity, ρ_f is the fluid density, and p is the pressure inside the fracture. The

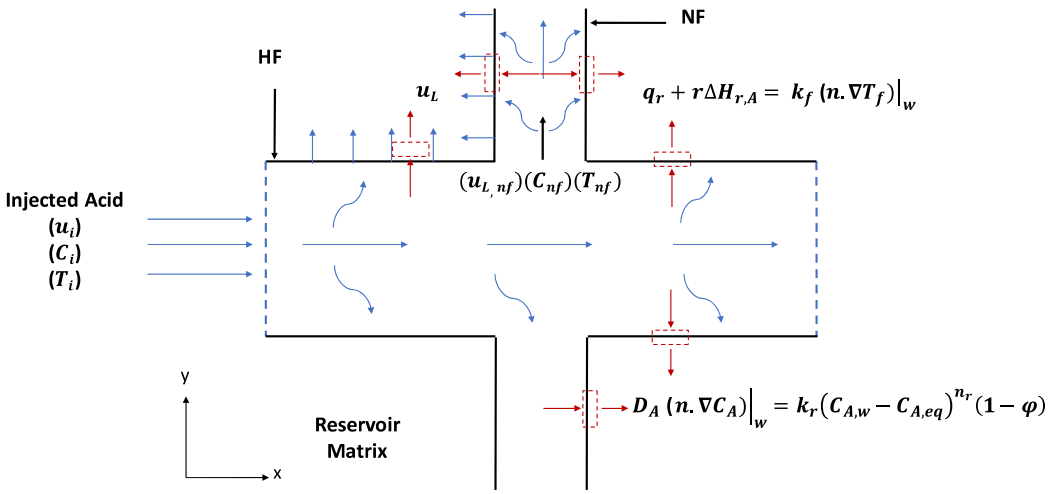

Fig. 3. Schematic showing the velocity, concentration, and temperature boundary conditions for the HF and NF.

velocity is obtained in the fracture length and width directions and assumed to be self-similar in the height direction. To obtain the velocity distribution inside the domain, the inlet (u_i, $u_{L,nf}$) and leakoff (u_L) velocities for both the HF and NFs should be specified (see Fig. 3). The leakoff velocity from the HF to the NF, $u_{L,nf}$, can be estimated as follows:

$$u_{L,nf} = \frac{1}{h_{nf}\,w_{nf}}\frac{\partial Q_{L,nf}}{\partial t} \tag{14}$$

The fracture propagation and flow models are then coupled with the acid reaction and heat transfer models. The acid reactive transport model is implemented to obtain the profile of acid concentration in the HF. The same methodology is used to estimate the acid reaction in NFs. The acid model can mathematically be described as:

$$\frac{\partial C_A}{\partial t} + \nabla.(\boldsymbol{u}C_A) = \nabla.(D_A\nabla C_A) \tag{15}$$

where C_A is the hydrochloric acid concentration, $\boldsymbol{u}$ is the velocity, D_A is the acid diffusion coefficient, and t is time. The first term in Eq. (15) accounts for acid accumulation, the second is the convection of acid, and the last is the diffusion term. The model assumes both convection and diffusion in the HF and NF length and width directions. Initially, the acid concentration in the domain is equal to zero. The reaction occurs at the domain boundary (i.e., fracture walls) and is handled as a boundary condition for both the HF and NFs (see Fig. 3).

$$D_A(\boldsymbol{n}.\nabla C_A)|_w = k_r\left(C_{A,w} - C_{A,eq}\right)^{n_r}(1-\varphi) \tag{16}$$

where $\boldsymbol{n}$ is the normal vector, k_r is the reaction rate constant, n_r is the reaction exponent, φ is the formation porosity, the subscript w stands for both HF and NFs walls, and the subscript eq stands for equilibrium. The equation states that the rate of acid diffusion is equal to the reaction rate at the fracture walls. The inlet acid concentration of the HF is the initial concentration, C_i, while the NF inlet concentration is the average HF concentration at the intersection point, C_{nf} (see Fig. 3).

The model is more precise when integrated with a temperature model, as the acid reactivity is a strong function of temperature, especially in cold dolomite rocks. The heat transfer model is written as:

$$\rho_f\widehat{c_{pf}}\left[\frac{\partial T_f}{\partial t} + \nabla.\left(\boldsymbol{u}T_f\right)\right] = \nabla.(k_f\nabla T_f) \tag{17}$$

where T_f is the fracture temperature, $\widehat{c_{pf}}$ is the specific fluid heat capacity, and k_f is the fluid thermal conductivity. The first term in Eq. (17) represents the heat storage, the second is heat convection due to fluid flow, and the last is heat conduction. Notice that the mathematical approach used to solve Eqs. (15) and (17) are similar. The heat of reaction and the heat flow from the reservoir are considered at the domain boundary and can be described as:

$$q_r + r\Delta H_{r,A} = k_f(n.\nabla T_f)|_w \tag{18}$$

where q_r is the heat flux from the reservoir, $\Delta H_{r,A}$ is the heat of reaction, and r is the reaction rate. Initially, the temperature in the domain is equal to the initial reservoir temperature, T_R. The inlet temperature of the HF is T_I while the NF inlet temperature is the HF average temperature at the intersection point (see Fig. 3). Notice that both the reaction rate constant and the diffusion coefficient depend on temperature according to the Arrhenius formula:

$$k_r = k_r^0 exp\left(-\frac{\Delta E}{RT}\right) \tag{19}$$

where k_r^0 is the pre-exponential factor, ΔE is the activation energy, R is the universal gas constant, and T is the absolute temperature. Similarly, the diffusion of fluids is a function of the temperature, according to the Arrhenius formula:

$$D = D_o exp\left(-\frac{\Delta E_D}{RT}\right) \tag{20}$$

where ΔE_D is the activation energy for the diffusion. The boundary states that the heat conducted towards the fracture wall is equal to the heat of reaction and heat flux from the formation. The heat flux from the reservoir can be described as:

$$q_r = \overline{k_e}(n.\nabla T_r)\big|_w \tag{21}$$

where $\overline{k_e}$ is the effective (rock and fluids) thermal conductivity and T_r is the reservoir temperature. To obtain the heat flux from the reservoir to the fracture, the heat transfer in the reservoir should be solved. The heat transfer in the reservoir can be described through the heat convection and conduction equation:

$$\overline{\rho\widehat{c_p}}\frac{\partial T_r}{\partial t} + \rho_f\widehat{c_{pf}}\boldsymbol{u}.\nabla T_r = \nabla.\left(\overline{k_e}\nabla T_r\right) \tag{22}$$

where $\overline{\rho\widehat{c_p}}$ is the average rock and fluid properties. The first term is the heat accumulation, the second term is the heat convection within the reservoir, and the final term is the heat conduction. Aljawad (2019) provided the methodology applied to couple the reservoir and HF heat transfer equations.

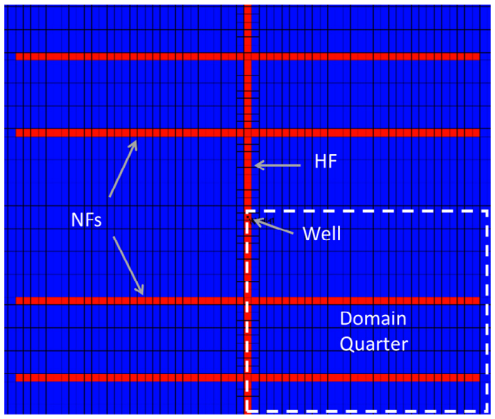

Fig. 4. Schematic of the domain used for reservoir production, including hydraulic and natural fractures.

The etched-width profiles of the HF and NFs are then obtained as follows:

$$\frac{\partial w_e}{\partial t} = \frac{\mathfrak{X}}{1-\varphi}\left(f_a u_L C_{A,w} - D_A \boldsymbol{n}.\nabla C_A|_w\right) \tag{23}$$

where w_e is the etched width by acid, f_a is the fraction acid lost that reacts at the fracture surfaces, and χ is the volumetric dissolving power. Then, the etched width is used to estimate the fracture conductivity, wk_f, profile based on the Nierode and Kruk correlation (1973) and presented as:

$$wk_f = \alpha e^{-\beta\sigma_c} \tag{24}$$

where α and β are constants and σ_c is the closure stress acting normal to the fracture surface.

In house reservoir simulator that simulates fluid flow in a fractured domain is used to estimate the productivity. This is accomplished by resolving the diffusivity equation, shown as:

$$\nabla \cdot (\boldsymbol{k} \cdot \nabla p) = \phi \mu_r c_t \frac{\partial p}{\partial t} \tag{25}$$

where p is the pressure, ϕ is the rock porosity, $\boldsymbol{k}$ is the permeability tensor, μ_r is the reservoir fluid viscosity, and c_t is total compressibility. The fracture permeability distributions for both HF and NFs are imported from the acid fracture model. Eq. (25) is solved to obtain the dimensionless productivity index at a pseudo-steady state. To solve the diffusivity equation above, the wellbore boundary condition can be described as a constant flow rate according to the following:

$$\left(\frac{\partial p}{\partial x}\right)_{wellbore} = -\frac{qB\mu_r}{\left(wk_f\right)_o 2h_{fo}} \quad at\ the\ wellbore \tag{26}$$

where q is production rate, $\left(wk_f\right)_o$ is wellbore-fracture contact conductivity, h_{fo} is the fracture height at the wellbore entrance, and B is the oil formation volume factor.

The distribution of HF and NFs are shown in Fig. 4. The wellbore is placed at the center and the HF extends in the north–south direction. NFs are assumed to be orthogonal to the HF and thus extend in the east–west direction. Due to symmetry, the simulation is only done on a quarter of the domain and the grids are refined towards the HF and NFs. The no-flow boundary condition is implemented everywhere within the reservoir quarter except at the wellbore:

$$\boldsymbol{n}.\nabla p = 0 \tag{27}$$

Simulation of the reservoir flow is done to estimate the productivity of the fractured well: for a certain treatment volume, the higher productivity scenario results from a better design. The productivity index can be defined as:

$$J = \frac{q}{\Delta p_{reservoir}} \tag{28}$$

where J is the productivity index, q is the production rate, and $\Delta p_{reservoir}$ is the reservoir drawdown. Fold of increase in productivity is used to compare different scenarios. Fold of increase represents the ratio of the fractured well productivity to the productivity before the acid fracturing, J_o.

3. Results and discussion

This section describes the following three steps taken in the present research. First, a productivity model decoupled from the acid fracture model was used to test the impact of NFs on productivity. Next, the impacts of NFs on acid fracturing and productivity improvement were analyzed. Finally, an optimization analysis was provided to determine the optimum design conditions when NFs exist at various reservoir permeability values. The data used in this study can be found in Tables 1–3. NFs were assumed to have the same height as the pay zone and the HF was contained within the targeted formation due to the large stress contrast between formation layers. The default size of the NFs was 20 ft in half-length and 0.005 in for the aperture; they were spaced every 20 ft away from the wellbore. It was also assumed that the NFs were subjected to 20% higher closure stress than was the HF. This is because the NF planes faced the maximum horizontal stress, according to the model.

3.1. Configuration of the conductive path

This section answers a fundamental question regarding the impact of the conductive path configuration. If the same fracture contact area and conductivity values are implemented in a reservoir simulator, will the distribution of the conductive path change the productivity? To resolve this question, two scenarios were tested. The first case contained only an HF, while the second contained one HF and five NFs in one quarter of the domain (see Fig. 4 for visualization). The fracture conductivity values (both HF and NF) were kept the same at 1000 md.ft. The contact areas were similar where the total fractures length was 1000 ft. This was done to keep everything similar except for the configuration of the conductive path. The first scenario had an HF with a 500 ft half-length. The other scenario included an HF with a 300 ft half-length and five NFs with 20 ft half-lengths each (40 ft in total length). Fig. 5 shows the difference between the two cases in terms of productivity improvement at different reservoir permeability values. The HF-only was superior in terms of productivity, especially at low reservoir permeabilities, despite similar contact areas and conductivities. Even though the conductive lengths were similar, the conductive lengths per quarter of the reservoir domain were smaller because only half the NFs were draining.

A third case was created to test if the total contact area per quarter of the domain would provide productivity levels like that of the HF case. Fig. 5 shows that the productivity of the third case (with a 40 ft NF half-length) was still lower than that of the HF-only scenario. This proved that the less efficient drainage associated with stimulated reservoir volume would be encountered with the HF intersecting NFs, which is interesting because similar contact areas and conductivity levels were assumed. This was because the NFs limited the length of the HF, leaving an untargeted section of the reservoir. This conclusion is especially important in tight formations where a long HF is desirable. Also, the HF was more efficient at draining the reservoir than were the NFs because it targeted a higher drainage volume.

Table 1
Input parameters used for the simulations.

Input data	SI unit	Field unit
Reservoir properties		
Formation pressure, P_r	2.3603×10^7 pa	3423 psi
Bottomhole pressure, P_w	1.0342×10^7 pa	1500 psi
Reservoir fluid density, ρ_f	855 kg/m^3	54.3 lb$_m$/ft^3
Formation length, L_x	1000 m	3280 ft
Formation width, L_y	1000 m	3280 ft
Reservoir fluid viscosity, μ_f	0.0012 kg/(m s)	1.2 cp
Formation volume factor, B	1.3	
Total compressibility, c_t	2.26×10^{-9} pa^{-1}	1.56×10^{-5} psi^{-1}
Reservoir temperature, T_R	100 °C	212 °F
Formation rock density, ρ_{ma}	2700 kg/m^3	168.48 lb$_m$/ft^3
Reservoir's rock specific heat capacity, c_{ma}	0.879 kJ/(kg °C)	0.2099 Btu(lb °F)
Reservoir's rock thermal conductivity, k_{ma}	1.57×10^{-3} kJ/(s m °C)	0.907 Btu/(h ft °F)
Formation depth, D	2408.5 m	7900 ft
Pay zone thickness, h	30.5 m	100 ft
Closure stress, σ_c	3.792×10^7 pa	5500 psi
Rock embedment strength, SRES	3.1×10^8	45,000 psi
Acid properties		
Density, ρ	1070 kg/m^3	66.77 lb$_m$/ft^3
Fracture fluid Injection rate, q_i	0.08 m^3/s	30 bpm
Power law exponent, n	0.90	
Power law consistency index, K	0.002 lb$_f$ s^n/ft^2	
Opening time distribution factor, κ	1.5	
Acid initial concentration, C_i	0.20 acid mass fraction	
Fracture fluid heat capacity, c_p	4.12 kJ/(kg °C)	0.962 Btu/(lbm °F)
Fracture fluid thermal conductivity, κ	6×10^{-4} kJ/(s m °C)	0.348 Btu/(h ft °F)
Fracture fluid temperature at injection, T_I	27 °C	80.6 °F

Table 2
Parameters for HCl acid and calcite minerals reaction (Schechter, 1992).

Mineral	n_r	k_r^0 [$\frac{\text{kg moles HCl}}{\text{m}^2\ \text{s}\ \left(\frac{\text{kg moles HCl}}{\text{m}^3\text{acid solution}}\right)^{n_r}}$]	$\frac{\Delta E}{R}$ (K)	ΔH_r ($\frac{\text{kJ}}{\text{mol HCl}}$)
Calcite	0.63	7.314×10^7	7.55×10^3	7.5

Table 3
Layers' geomechanical properties; perforations exists in layer 2.

Layer number	Top of layer (ft)	Layer thickness (ft)	Stress (psi)	Toughness (psi inch$^{0.5}$)	Young's modulus (psi)
1	0	7900	6500	2000	6.0×10^6
2	7900	100	5500	2000	6.0×10^6
3	8000	100	6500	2000	6.0×10^6

3.2. Impact of NFs on acid fracturing

A dynamic acid fracture model was used to generate HF and NF permeabilities. It was determined that the larger the number and size of NFs in the formation, the smaller the size of the HF. A case was generated to compare the acid fracturing of a carbonate formation with no NFs to another with NFs spaced 20 ft from the HF; each had a 20 ft half-length. For the sake of simplicity, the NFs were assumed to be perpendicular to the HF and dilated once the HF reached the location of the intersection. In this case, 1500 bbl of 20% wt. retarded HCl injected at 30 bpm was simulated for the two scenarios. The selection of the treatment volume, type, and acid concentration was based on current field designs.

Fig. 6 shows the location of the HF (only the half-length) in the quarter of the reservoir; the original location represents the wellbore. The figure shows only a portion of the simulation domain (of the quarter). In this case, the fracture half-length was simulated, reaching 440 ft where the acid concentration gradually dropped along the HF (see Fig. 6). When the NFs were introduced into the model, the length of the HF was reduced to 235 ft (see Fig. 7). Even though the HF length was reduced, the total acidized area was larger with the NFs.

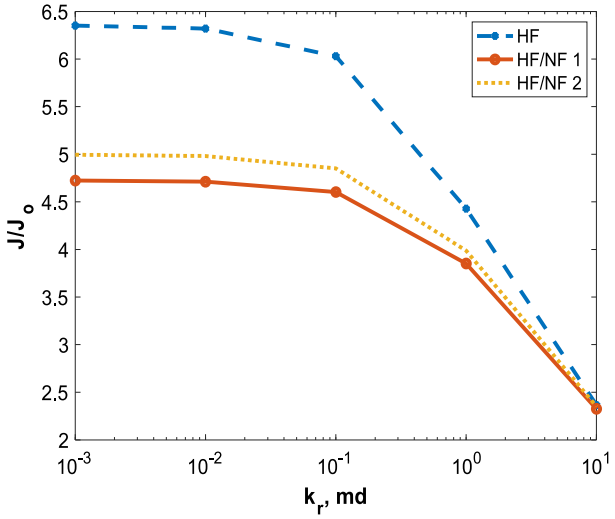

Fig. 5. Productivity comparison of the two scenarios at different reservoir permeabilities, assuming similar conductivities and contact areas.

Fig. 8 shows the etched width along the HF. As can be observed, most of the dissolution occurred near the wellbore and gradually dropped along the HF. This behavior is common when HCl is used to dissolve an HF in a calcite formation. Fig. 9 shows the dissolution pattern when NFs were introduced. The largest etched width occurred near the wellbore and at the intersection locations. This was because the NF aperture was very small (0.005

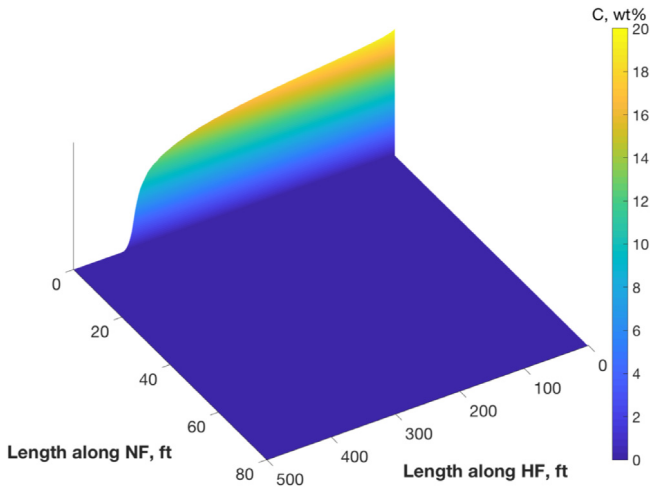

Fig. 6. Acid concentration distribution along the hydraulic fracture.

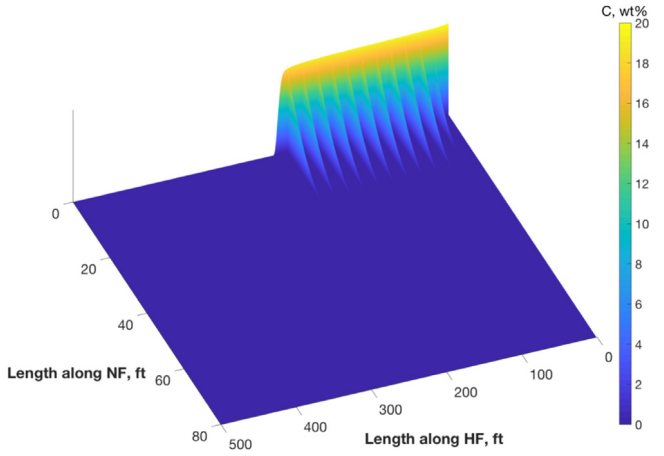

Fig. 7. Acid concentration distribution along both the hydraulic and natural fractures.

in). This significantly reduced the Peclet number ($N_{pe} = \frac{u_L w}{2D_A}$), resulting in a fast acid reaction at the intersection. It should be noted that the fracture width is updated at each time step by adding the etched width. Also, the further away the NFs were from the wellbore, the lower the etching magnitude and shorter the penetration lengths in the NFs. This was logical, as the acid was being consumed while traveling, resulting in less etching in the NFs further from the wellbore.

One fundamental question concerned the impact of NFs on the productivity of acid fracture wells. To answer this question, a permeability distribution was generated based on the etching profile. The etching profile was converted into conductivity distribution using the Nierode–Kruk correlation. It was then exported to the reservoir model as a permeability distribution. Fig. 10 shows the permeability distribution of the HF case, while Fig. 11 shows the permeability distribution of the NF case. Notice that the natural logarithmic of the permeability is shown in each to make visualization possible. The productivity improvement in the HF-only case was 6.0, while it was approximately 4.4 in the NF case, assuming a 0.01 md reservoir permeability. One possible reason for the lower productivity is that the NFs caused the HF to be significantly shorter. Hence, depletion was restricted to a shorter distance within the wellbore. Also, NFs are subject to higher closure stress, which causes them to lose conductivity along a sharper gradient than what is seen in HFs.

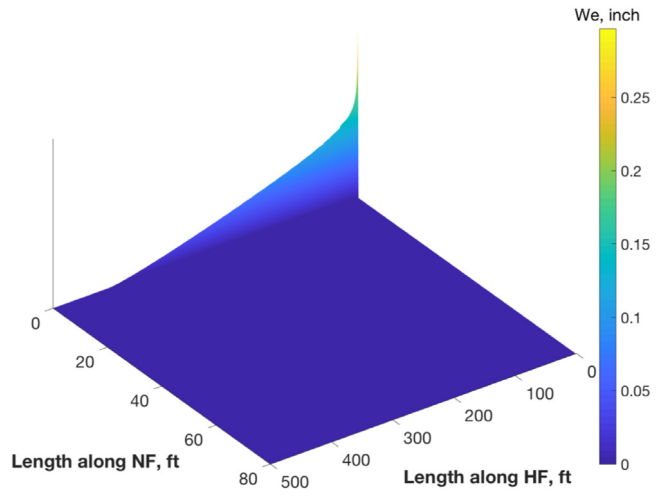

Fig. 8. Etched-width distribution along the hydraulic fracture.

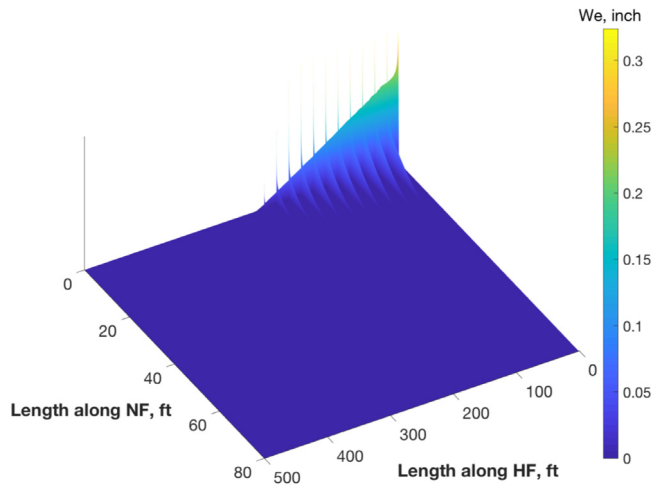

Fig. 9. Etched-width distribution along both the hydraulic and natural fractures.

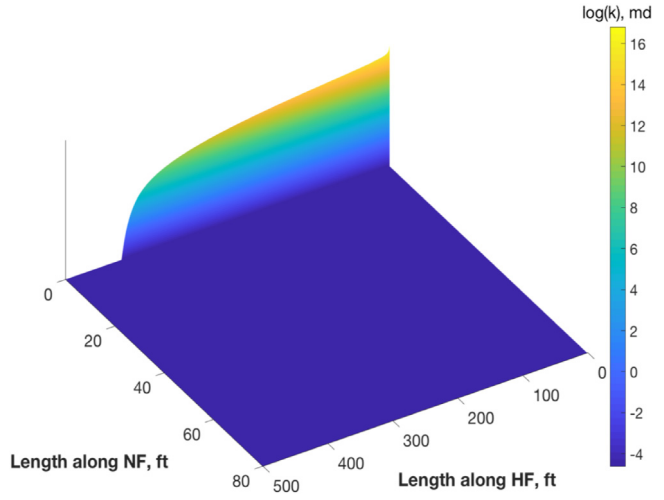

Fig. 10. Permeability distribution along the hydraulic fracture.

A sensitivity analysis was conducted to determine the impact of NF properties on the productivity of acid fractured wells. The number of NFs was determined from the spacing, with lower

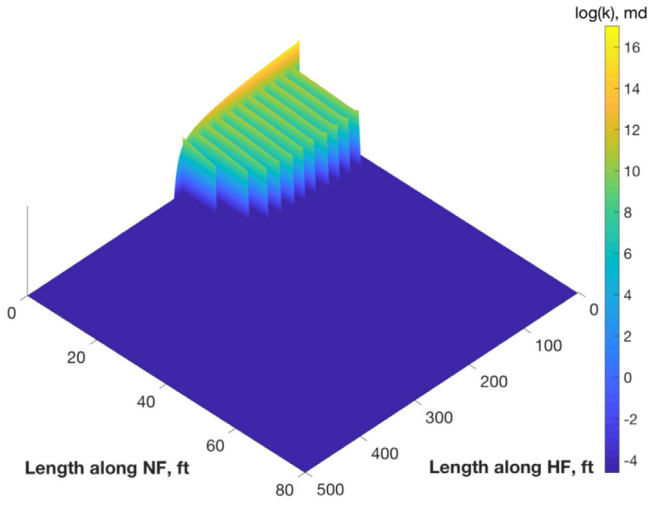

Fig. 11. Permeability distribution along both the hydraulic and natural fractures.

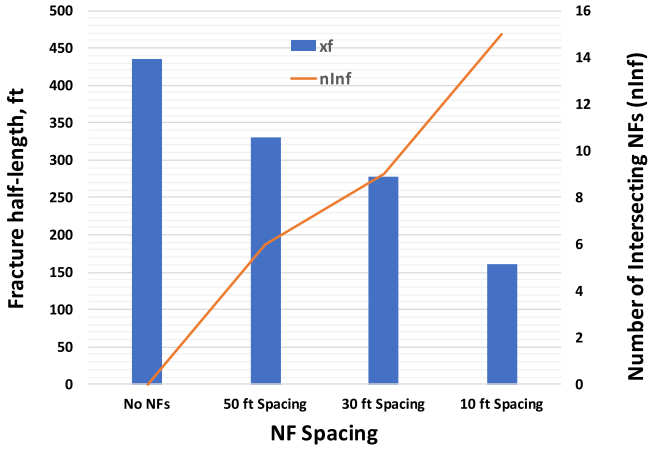

Fig. 12. Impact of NF spacing on the hydraulic fracture half-length and number of intersecting natural fractures.

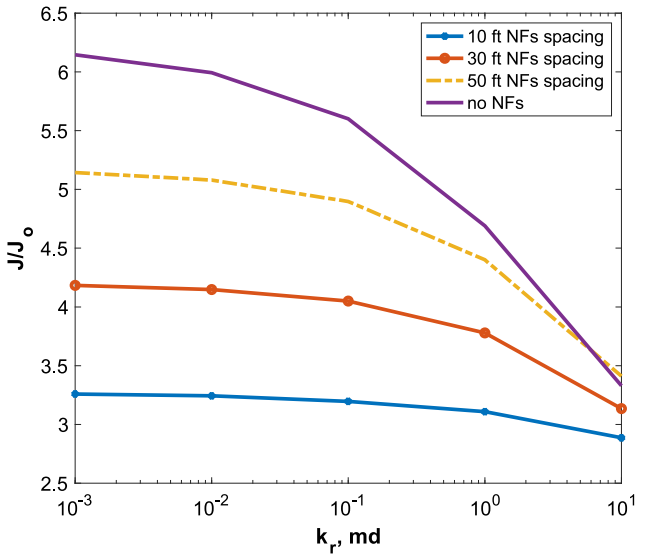

Fig. 13. Impact of NF spacing on productivity improvement at different reservoir permeabilities.

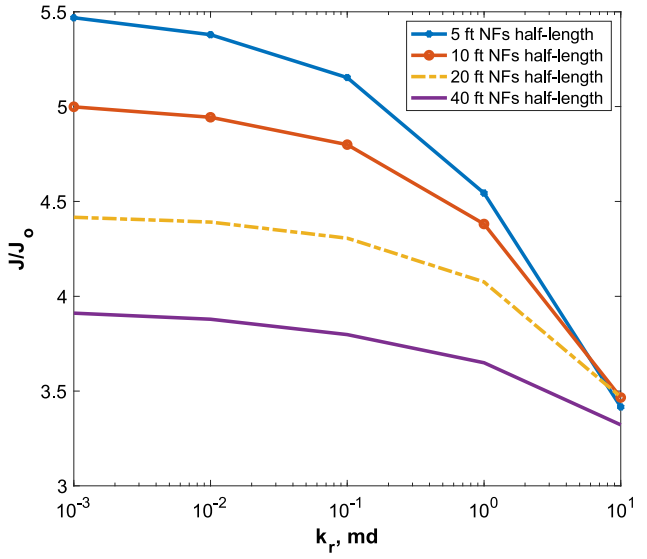

Fig. 14. Impact of NF length on productivity improvement at different reservoir permeabilities.

spacing meaning more NFs. The larger the number of NFs was, the lower the HF length became, due to excessive fluid loss. Fig. 12 shows the inverse relationship between spacing and hydraulic fracture length. It also shows that when the NF spacing was short, the HF intersected more NFs, which was a logical outcome and significantly impacted the productivity of the fractured well. Fig. 13 shows the impact of NF spacing on productivity at different reservoir permeabilities. It can be observed that the shorter the NF spacing, the lower the productivity. The impact was more significant at lower reservoir permeabilities. At higher reservoir permeabilities, fracture conductivity was what controlled productivity. The existence of NFs did not reduce the conductivity significantly, and hence the NFs had almost no impact. Nevertheless, HF length is a very significant parameter when the reservoir permeability is low. That is why the HF-only case was better when a long HF length was generated. Therefore, using diverters to reduce fluid loss is a very important technique when acid fracturing a naturally fractured carbonate formation.

Another parameter that was analyzed was NF length. A constant spacing (20 ft in this case) was assumed, and it was found that the longer the NF length, the lower the HF length and level the productivity was reduced (see Fig. 14). Again, this impact was more significant at lower reservoir permeabilities.

Finally, the impact of the initial NF width on productivity was investigated, assuming all other aspects were constant. As Fig. 15 shows, the initial NF widths had almost no impact on productivity when the NFs width was lower than 0.1 in. In that range, the etched width controlled acid distribution and conductivity once the acid reacted with the NFs. This occurred as the etched width at the intersection was orders of magnitude larger than the initial NFs width. When the NFs width was larger than 0.1 in, its impact on productivity was more significant. The fluid loss from the HF to the NFs increased, reducing the HF length and hence the fractured well productivity. The impact was more prominent at the lower range of reservoir permeability; a situation where larger HF length is desired. Such large NFs width is possible in vuggy carbonate formations.

Fig. 16 shows the etched width distribution along the HF and NFs assuming 0.5 in NF width. The figure shows no dissolution spikes at the intersection points as was observed for the 0.005 in NF width (see Fig. 9). That was the case for all the scenarios where the NF width was larger than 0.1 in. In these cases, the etched width is only a fraction of the initial NF width as the

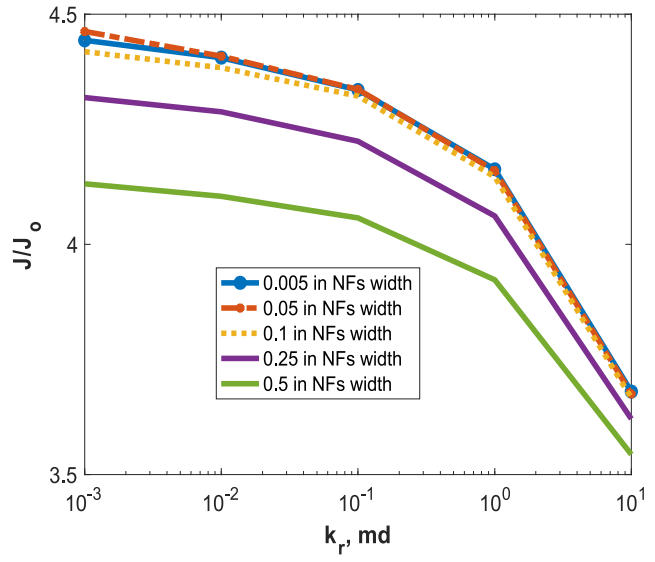

Fig. 15. Impact of NF width on productivity improvement at different reservoir permeabilities.

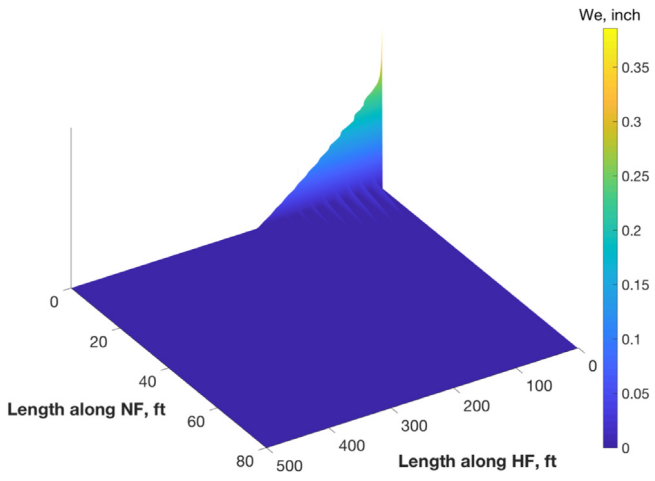

Fig. 16. Etched-width distribution along both the hydraulic and natural fractures for 0.5 in NFs width.

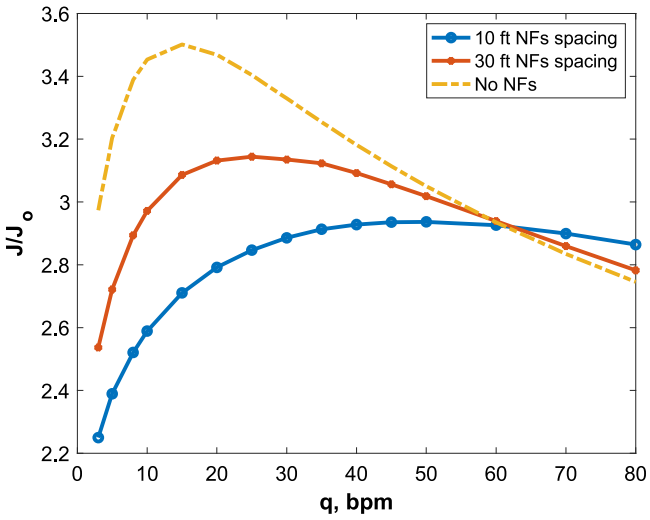

Fig. 17. Optimum acid injection rate at different NF spacings and a 10 md reservoir permeability.

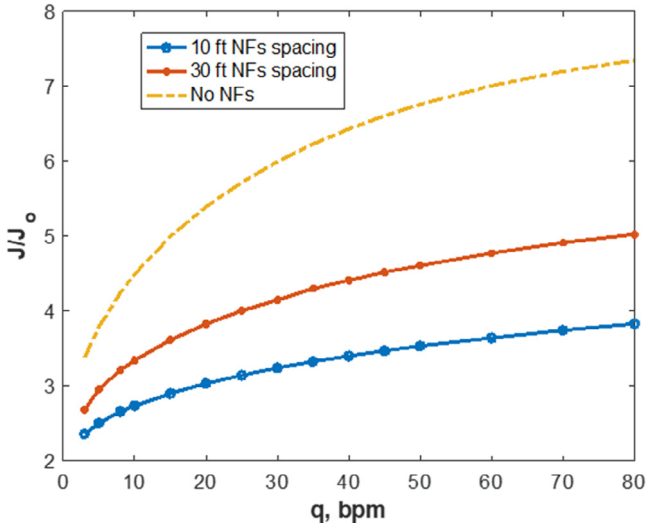

Fig. 18. Optimum acid injection rate at different NF spacings and a 0.01 md reservoir permeability.

Peclet number was large which reduced the reaction rate at the intersections.

3.3. Design optimization

The impact of NF intensity (i.e., spacing) on the optimum acid injection rate was also investigated. The optimum design is the one that gives the maximum productivity for a given treatment volume. The input of acid and reservoir properties (see Tables 1–3) were implemented, as well as the default NF half-length (20 ft) and width (0.005 in). This study was based on a constant treatment volume of 1500 bbl of 20% retarded HCl. Design optimization was conducted at low and moderate reservoir permeabilities.

3.3.1. Moderate reservoir permeability (10 md)

At moderate reservoir permeabilities, creating a short and highly conductive fracture path was favorable to creating a long fracture with low conductivity. Fig. 17 shows the productivity improvement in a fractured well at different injection rates and NF spacing. The optimum productivity achieved with no NFs was higher than with 10 ft and 30 ft NF spacing. Additionally, the optimum injection rate increased with an increase in NF intensity. Fig. 17 shows that the optimum injection was 15 bpm for no NFs, 20 bpm for 30 ft spacing, and between 40 and 70 bpm for 10 ft spacing. Reaching the optimum HF length is challenging when NFs exist and hence, the injection rate should be increased.

3.3.2. Low reservoir permeability (0.01 md)

Low reservoir permeability favors the creation of long fractures. High injection rates are usually associated with lower fluid loss rates and larger fracture sizes. Fig. 18 shows that the productivity was significantly higher in the formation not containing NFs. The greater the number of NFs in the formation, the lower the productivity that was seen. The optimum injection rate, however, was at the maximum for all cases. It was also concluded that using larger volumes of pad and diverters would help improve productivity significantly, as they both increase HF size.

4. Conclusion

A dynamic acid fracture and productivity model that considers the existence of NFs was developed for this research. It was found not only that the fracture contact area and conductivity determined productivity, but also the configuration of the conductive path. The existence of NFs harmed productivity as compared to the formation with no NFs. It was observed that the larger the intensity and length of the NFs, the lower the productivity of the acid fractured wells. Also, if the NFs width is relatively large, it negatively impacted the productivity by reducing the size of the HF due to the excessive fluid loss. An optimization study was conducted at low and moderate reservoir permeabilities, demonstrating that the optimum acid injection rate at moderate reservoir permeabilities increased with increases in NF intensity. However, the maximum injection rate should be targeted at low reservoir permeabilities, no matter the intensity of the NFs.

Declaration of competing interest

The authors declare that they have no known competing financial interests or personal relationships that could have appeared to influence the work reported in this paper.

CRediT authorship contribution statement

Murtada Saleh Aljawad: Conceptualization, Methodology. **Mateus Palharini Schwalbert:** Methodolgy. **Mohamed Mahmoud:** Investigation. **Abdullah Sultan:** Investigation.

Acknowledgment

The authors would like to acknowledge KFUPM, Saudi Arabia for supporting this study under grant # SR181004.

References

Abass, H.H., Al-Mulhem, A.A., Alqam, M.H., Khan, M.R., 2006. Acid fracturing or proppant fracturing in carbonate formation? A rock mechanics view. In: SPE Annual Technical Conference and Exhibition. Society of Petroleum Engineers, http://dx.doi.org/10.2118/102590-MS.

Agrawal, S., Shrivastava, K., Sharma, M.M., 2019. Effect of shear slippage on the interaction of hydraulic fractures with natural fractures. In: SPE Hydraulic Fracturing Technology Conference and Exhibition. Society of Petroleum Engineers.

Aljawad, M.S., 2019. Identifying formation mineralogy composition in acid fracturing from distributed temperature measurements. SPE Reserv. Eval. Eng..

Aljawad, M.S., Aljulaih, H., Hughes, B., Desouky, M., 2019a. Integration of field, laboratory, and modeling aspects of acid fracturing: A comprehensive review. J. Pet. Sci. Eng..

Aljawad, M.S., Palharini Schwalbert, M., Zhu, D., Hill, A.D., 2019b. Optimizing acid fracture design in calcite formations: Guidelines using a fully integrated model. SPE Prod. Oper..

Aljawad, M.S., Schwalbert, M.P., Zhu, D., Hill, A.D., 2020. Improving acid fracture design in dolomite formations utilizing a fully integrated acid fracture model. J. Pet. Sci. Eng. 184, 106481.

Berman, A.S., 1953. Laminar flow in channels with porous walls. J. Appl. Phys. 24 (9), 1232–1235.

Hill, A.D., Zhu, D., Wang, Y., 1995. The effect of wormholing on the fluid loss coefficient in acid fracturing. SPE Prod. Facil. 10 (04), 257–264.

Li, Y., Sullivan, R.B., de Rozieres, J., Gaz, G.L., Hinkel, J.J., 1993. An overview of current acid fracturing technology with recent implications for emulsified acids. In: SPE Annual Technical Conference and Exhibition. Society of Petroleum Engineers.

Liu, S., Valkó, P.P., 2018. A rigorous hydraulic-fracture equilibrium-height model for multilayer formations. SPE Prod. Oper. 33 (02), 214–234.

Mou, J., Li, C., Zhang, S., Li, D., 2016. Research on acid leakoff reduction by injecting large volume of slick water in acid fracturing of naturally fractured oil reservoirs. Oxid. Commun. 39 (3 A), 2566–2579.

Nierode, D.E., Kruk, K.F., 1973. An evaluation of acid fluid loss additives retarded acids, and acidized fracture conductivity. In: Fall Meeting of the Society of Petroleum Engineers of AIME. Society of Petroleum Engineers, http://dx.doi.org/10.2118/4549-MS.

Palharini Schwalbert, M., Aljawad, M.S., Hill, A.D., Zhu, D., 2020. Decision criterion for acid stimulation method in carbonate reservoirs: Matrix acidizing or acid fracturing? In: SPE International Conference and Exhibition on Formation Damage Control. Society of Petroleum Engineers.

Potluri, N.K., Zhu, D., Hill, A.D., 2005. The effect of natural fractures on hydraulic fracture propagation. In: SPE European Formation Damage Conference. Society of Petroleum Engineers.

Ravikumar, A., Marongiu-Porcu, M., Morales, A., 2015. Optimization of acid fracturing with unified fracture design. In: Abu Dhabi International Petroleum Exhibition and Conference. Society of Petroleum Engineers, http://dx.doi.org/10.2118/177486-MS.

Schechter, Robert S., 1992. Oil Well Stimulation. Prentice-Hall, Inc., Englewood Cliffs, New Jersey.

Schwalbert, M.P., 2019. Comprehensive Analysis of Acid Stimulation in Carbonates (Ph.D. Dissertation). Texas A & M University, College Station, Texas, USA.

Sevougian, S.D., Schechter, R.S., Sepehrnoori, K., 1987. Optimization of vertical acid fractures in steady-state flow. In: SPE International Symposium on Oilfield Chemistry. Society of Petroleum Engineers, http://dx.doi.org/10.2118/16252-MS.

Ugursal, A., Schwalbert, M.P., Zhu, D., Hill, A.D., 2018. Acid fracturing productivity model for naturally fractured carbonate reservoirs. In: SPE International Hydraulic Fracturing Technology Conference and Exhibition. Society of Petroleum Engineers, http://dx.doi.org/10.2118/191433-18IHFT-MS.

Wu, K., Olson, J.E., 2016. Numerical investigation of complex hydraulic-fracture development in naturally fractured reservoirs. SPE Prod. Oper. 31 (04), 300–309.